Bulletin of the Seismological Society of America, Vol. XX, No. XX, pp. –, – 2019, doi: 10.1785/0120190037

Ⓔ

κ_0 and Broadband Site Spectra in Southern California from Source Model-Constrained Inversion

by Alexis Klimasewski,* Valerie Sahakian, Annemarie Baltay, John Boatwright,† Jon B. Fletcher, and Lawrence M. Baker

Abstract Ground-motion modeling requires accurate representation of the earthquake source, path, and site. Site amplification is often modeled by V_{S30}, the time-averaged shear-wave velocity of the top 30 m of the Earth's surface, though recent studies find that its ability to accurately predict site effects varies. Another measure of the site is κ_0, the attenuation of high-frequency energy near the site (Anderson and Hough, 1984). We develop a novel application of the Andrews (1986) method to simultaneously invert the spectra of 3357 earthquakes in Southern California into source and site components. These earthquakes have magnitudes 2.5–5.72 and were recorded on 16 stations for a total of 52,297 records. We constrain the inversion with an individual earthquake, demonstrating the most Brune-like shape to preserve the site spectra. We then solve for κ_0 site amplification at each station in three frequency bands: 1–6 Hz, 6–14 Hz, and 14–35 Hz. The resulting values of κ_0 range from 0.017 s at ANZA station PFO to 0.059 s at ANZA station SND. We compare our results to values of site κ_0 from other studies, as well as site residuals from ground-motion prediction equations. We find good agreement between our site κ_0 and previous studies in the region. We find that κ_0 and high-frequency site amplification (14–35 Hz band) correlates well with independent site residuals, making it a good first-order approximation for the effects of site attenuation or amplification on ground motion.

Supplemental Content: Table and figures showing individual site spectra and their V_{S30} values and the relationship between V_{S30} and ground-motion prediction equation (GMPE) site residuals.

Introduction

Recorded ground motion is often considered by both seismologists and engineers to have three basic components: the earthquake source, the recording site, and the path between the two. Seismologists often deconvolve these three components to study the earthquake source (Allmann and Shearer, 2009; Trugman and Shearer, 2018), site (Castro *et al.*, 1990; Boatwright *et al.*, 1991; Kilb *et al.*, 2012), or path (Hough *et al.*, 1988; Oth *et al.*, 2011; Sahakian *et al.*, 2018). Ground-motion prediction equations (GMPEs) parameterize the same source, path, and site components in empirical models. The engineering community relies on accurate estimation of recorded ground motion for hazard calculations or design of critical facilities. In a hazard calculation, the source parameters for a particular future earthquake (besides the general faulting dimension and magnitude) are difficult to estimate. However, regional path and site effects can be estimated *a priori* and should be stable over time and therefore built into ground-motion models. Site conditions are a fundamental component of ground-motion models, describing how much amplification can be expected at a site.

There are a variety of methods used to characterize site amplification. V_{S30}, the time-averaged shear-wave velocity of the top 30 meters of the Earth's surface, is commonly used to describe site amplification (Douglas, 2002), though recent studies find that its ability to accurately predict site effects varies (Gallipoli and Mucciarelli, 2009; Yong *et al.*, 2012; Derras *et al.*, 2016, 2017; Thompson and Wald, 2016; Sahakian *et al.*, 2018). Other parameters that can be derived empirically may perform better as predictors of site amplification. κ_0, the attenuation of high-frequency energy near a site, has been found to be a promising measure of site effects because it correlates well with both higher frequency ($5 < f < 10$ Hz) ground motion and peak ground acceleration (PGA; Silva and Darragh, 1995; van Houtte *et al.*,

*Now at the Department of Earth Sciences, University of Oregon, Eugene, Oregon 97403 U.S.A.

†Deceased (2018).

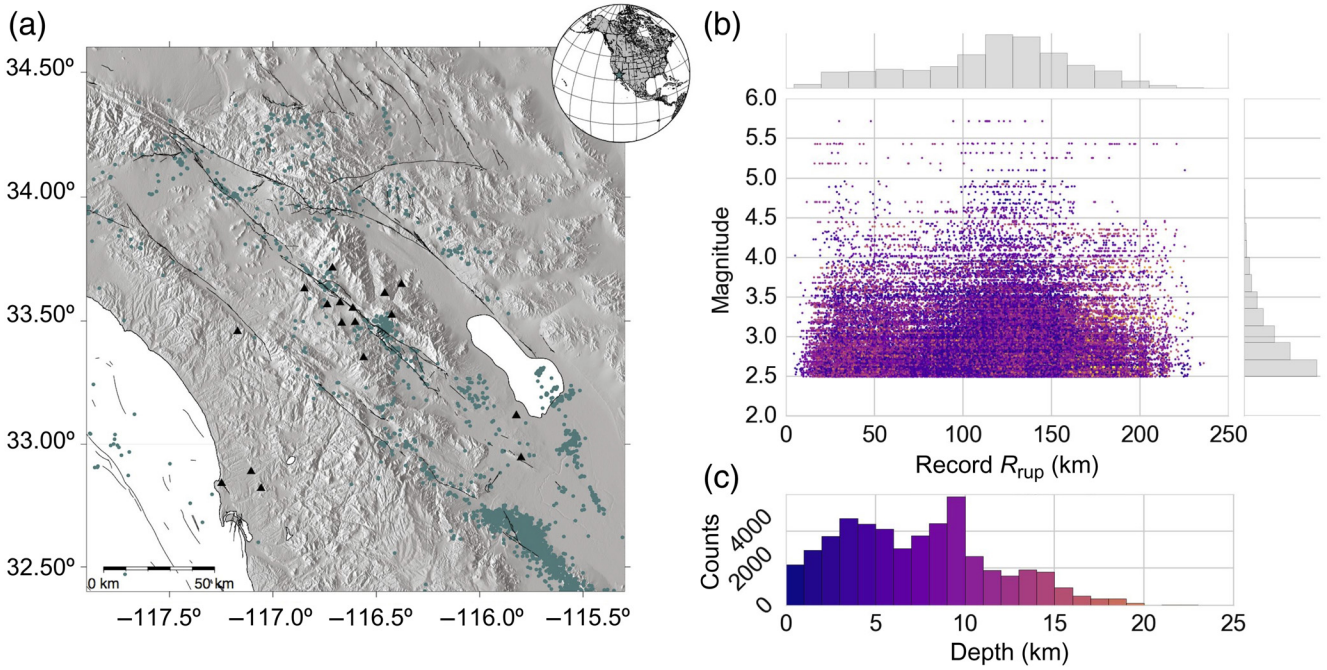

Figure 1. (a) Study region with event locations (dots) and stations (triangles). (b) Magnitude distance plot for all 52,297 record paths in our sample, shaded by event hypocentral depth; for our small-magnitude events we approximate $R_{rup} = R_{hyp}$. Histograms of distance (above) and magnitude (right) are also shown on the plot. (c) Histogram of event hypocentral depths for all 3357 events in the sample. The color version of this figure is available only in the electronic edition.

2014). Because of its applicability, κ_0 has gained attention in the engineering community and is present in some GMPEs as a site term (Laurendeau *et al.*, 2013; Ktenidiou *et al.*, 2014). In reality, a combination of parameters may be the best way to fully capture site effects on ground motions. The full site spectrum is a more complete description of the attenuation and amplification at a site, making it potentially useful in both seismological applications and ground-motion models.

We use a novel method to decompose record spectra into source and site spectra, using a modified version of the Andrews (1986) decomposition method, with a Brune spectral constraint. Andrews (1986) constrained his inversion of 67 Mammoth Lakes earthquakes to a reference site to calculate broadband site spectra, of interest to constraining site response. This is important because the variability in site response can have a greater effect on ground-motion uncertainties than variations in source excitation (stress drop). Here, we focus on presenting the site spectra and the parameters that govern them. As opposed to common methods of computing κ_0 that typically measure κ on individual records and solve for the distance dependence back to κ_0, our method allows us to directly derive both κ_0 from the site spectra, as well as other spectral parameters, such as spectral amplification in various frequency bands. We simultaneously invert more than 50,000 shear-wave record spectra from earthquakes in southern California and explore the resulting spectral parameters. We compare our results to empirical values of site amplification from other studies, as well as site residuals from GMPEs. Our method also results in absolute site spectra for all 16 sites considered in southern California, which is useful for building site-specific GMPEs.

Methods

Earthquake Dataset

The data in this study consist of earthquakes magnitude 2.5–5.72 occurring between 2010 and 2016 in southern California (Fig. 1a). We use data from 15 ANZA network stations: BZN, CPE, CRY, FRD, KNW, LVA2, PFO, RDM, SMER, SND, SOL, TRO, WMC and three California Institute of Technology (Caltech) network stations: ERR, PMD, SWS (California Institute of Technology [Caltech], 1926; Berger *et al.*, 1984; Vernon, 1989; Southern California Earthquake Data Center [SCEDC], 2013). Our data include 52,297 records of 3357 earthquakes. Many of our events are aftershocks of the April 2010 El Mayor–Cucapah **M** 7.2 earthquake, but we include events over a larger geographic area to have more paths and stations sampled. The depths of the events range from 0 to 28.7 km, with more than 99% of events shallower than 20 km (Fig. 1b). Our data include records with closest distance to rupture R_{rup} of 4.4–235.8 km, with a median distance of 121.8 km. Because all our events are relatively small and can be assumed to be point sources, we approximate R_{rup} as R_{hyp}. All records are from three-component broadband (100 Hz sampling rate) instruments.

Each of the 3357 events is recorded at almost every one of the 16 stations in our database, yielding a robust dataset to use in inverting for site spectra. We use horizontal components

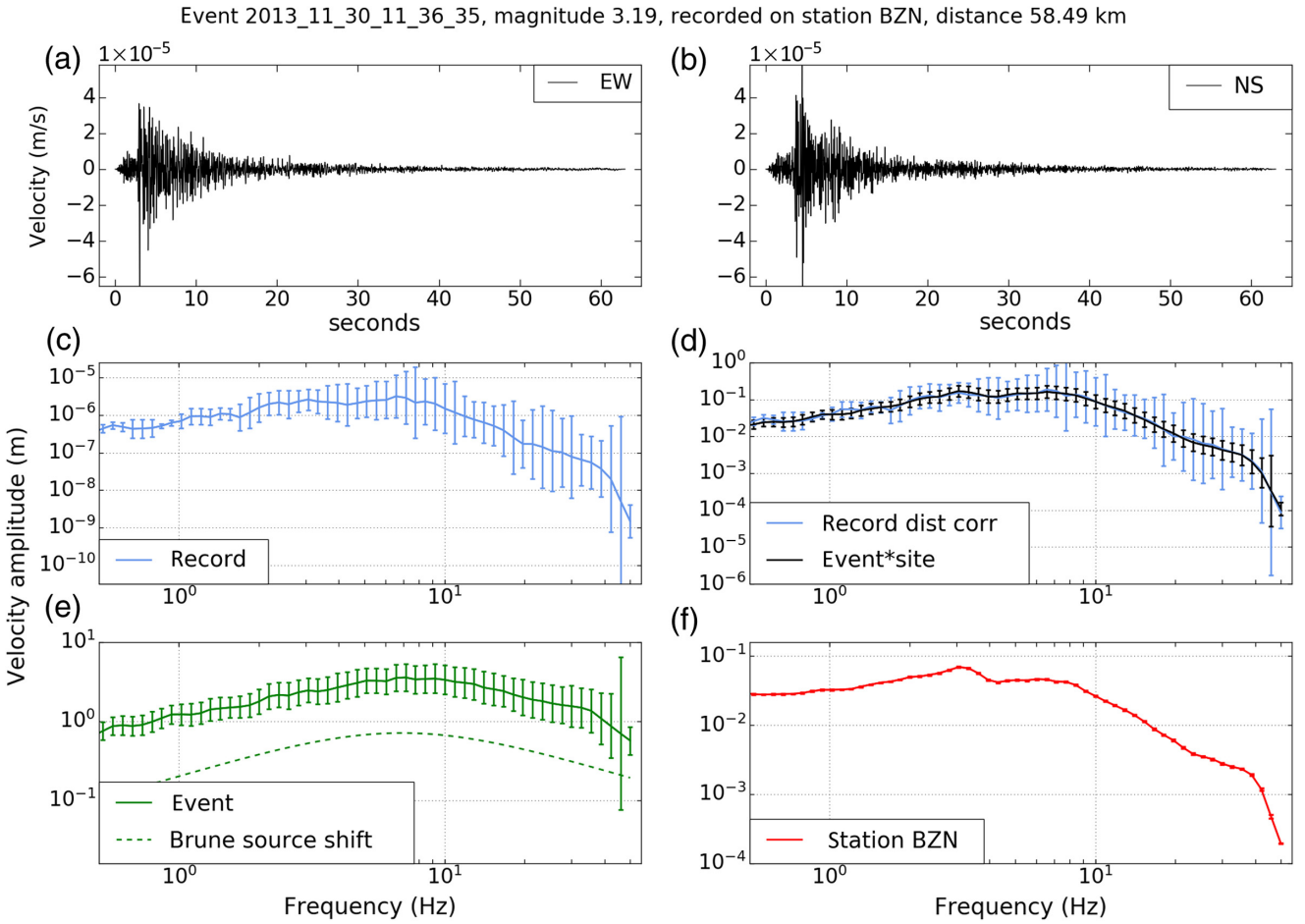

Figure 2. (a) Waveforms from the east–west (EW) and (b) north–south (NS) components for a magnitude 3.19 earthquake 2013_11_30_11_36_35 recorded on Station BZN at a distance of 58.49 km. The waveforms are cut at 2 s before the theoretical *S*-wave arrival and 60 s after. (c) Velocity spectrum for this recording, prior to correcting for distance. (d) Observed spectrum, after correcting for geometric spreading (lighter line) and inversion prediction (darker line). (e) Unconstrained event spectrum from the inversion (solid line) and the theoretical Brune spectrum (dashed line). (f) Unconstrained site spectrum from the inversion. Each spectrum is plotted with 1 sigma error bars in each frequency bin. The color version of this figure is available only in the electronic edition.

of the broadband seismograms and cut each record to start 2 s before and 60 s after the theoretical shear-wave arrival to capture the shear-wave signal, calculated using event time, propagation distance, and a regional average crustal velocity of 3.5 km/s. We also tested a shorter 15 s window and found that κ_0 are slightly higher (most sites within 5%), and our conclusions remain the same. We choose the 60 s window after the arrival to fully resolve the lower frequencies. We correct for instrument response and apply an antialiasing band-pass, cosine-tapered filter from 0 to 0.001 Hz and 35 to 50 Hz (Fig. 2a). The Fourier spectra for each shear-wave cut record were computed using the mtspec Python wrapper for the Multitaper Spectrum Estimation Library (Prieto *et al.*, 2009). The multitaper method is the minimum variance estimate for computing spectra introduced by Thomson (1982) as an alternative to a simple Fourier transform and smoothing. We use seven multitapers including a quadratic taper (Prieto *et al.*, 2007). We then average the record spectra of the two horizontal components, and discretize this spectrum in 75 frequency bins with equal logarithmic spacing between 0.1 and 50 Hz.

We use the 5% and 95% jackknife-sampled confidence intervals from mtspec to compute the uncertainties on our shear-wave spectra. We assume that errors are normally distributed and use a z score of 1.645 (90% confidence) to calculate 1 sigma error bars for each point in the spectra. We set the variance in each bin to the maximum error of all points in the bin (Fig. 2c).

V_{S30} values (Ⓔ Table S1, available in the supplemental content to this article, as reported by Sahakian *et al.*, 2018) for four of our 16 stations were measured using the multichannel analysis of surface waves method by Yong *et al.* (2016); the other 12 stations have proxy V_{S30}s calculated using the terrain-based proxy method of Yong *et al.* (2016).

Inversion for Source and Site Spectra

To decompose record spectra into source and site contributions, we adapted the method developed by Andrews

(1986) (equation 1), which allows us to preserve spectra for all stations in the dataset. Andrews (1986) modeled the record power spectra ($R(f)$), corrected for $1/R$ geometrical spreading, as the product of the source ($E(f)$) and site ($S(f)$) power spectra as functions of frequency (f) (Fig. 2c). The equation is linearized by taking the logarithm

$$\log(R_{ij}(f)^2) = \log(E_i(f)^2) + \log(S_j(f)^2), \qquad (1)$$

for every record with event i and station j, for a total of $i \times j$ equations for each of the 75 frequency bands. We solve for the generalized inverse solution of this equation simultaneously in each discrete frequency bin for all 52,297 records to determine each site and source spectrum (Fig. 2e,f).

We calculate uncertainties on our site and source spectra using the generalized inverse solution for the covariance matrix. We find the covariance of the data from the confidence intervals that result from mtspec, during computation of the spectra. The multitaper method of mtspec is the minimum variance method for obtaining spectra and produces 5% and 95% confidence intervals. Assuming a Gaussian distribution in the data, we find the 1 sigma error on each point of the spectra using a z score of 1.645 for the inner 90% of the error distribution. We then populate the data covariance matrix of the spectral decomposition inversion with the variance from mtspec, assuming that this represents variations in the spectral data. We assume that the data are independent and uncorrelated, so all covariances are zero, and the matrix is diagonal. Finally, to obtain the model covariance (on the resulting event and site spectra), we propagate this uncertainty through in the inversion using the following equation, from Aster *et al.* (2004):

$$\mathrm{Cov}(\boldsymbol{m}_\dagger) = \boldsymbol{G}^\dagger \mathrm{Cov}(\boldsymbol{d})(\boldsymbol{G}^\dagger)^T, \qquad (2)$$

in which $\mathrm{Cov}(\mathbf{d})$ is the data covariance, $\mathrm{Cov}(\mathbf{m}_\dagger)$ is the generalize inverse solution, and $\mathbf{G}^\dagger$ is the pseudoinverse of the forward problem matrix, as defined in our inversion.

The uncertainties on the record spectra are larger than the combined uncertainties on the resulting site and event spectra because the inversion is minimizing the square of the errors, the L2 norm (Fig. 2d). The site spectra all have very small uncertainties compared with the event spectra, likely because we have many more events than sites, and so the inversion minimizes the uncertainties on the site spectra much more than the event spectra (Fig. 2e,f).

This inversion method outputs source and site spectra, relative to each other, so there is an extra degree of freedom in our results, necessitating a constraint function. Any function of frequency can be added or subtracted to the source spectra and subsequently subtracted or added to the site spectra to result in the same record spectra. Previous work with the Andrews decomposition method (e.g., Andrews, 1986; Boatwright *et al.*, 1991) constrained the results using a reference site or sites, wherein the reference site spectra or average site spectra was subtracted from all other site spectra and added to all source spectra (in logarithmic space). However, using reference sites only allows each site spectra to be analyzed compared to the other and renders the spectra of the reference site unusable. Instead of using a reference site, our approach is to constrain the inversion using the deviation of a single constraint identifying event (CIE) away from a modeled Brune spectrum. With this constraint function, our constrained site spectra are relative to the inversion method and data but are able to more completely describe site behavior without losing the response of a reference site. Furthermore, site spectra are typically not well known, as compared with a basic functional form (model) for earthquake source spectra.

Computing our constraint function first requires finding a CIE that exhibits the most "Brune-like" spectral shape (Brune, 1970, 1971) out of all events in the dataset and then using the difference between the CIE spectrum and the theoretical spectrum as the constraint function. To search for the CIE, we use a regional stress drop of 5 MPa (i.e., Atkinson and Silva, 2000; Baltay and Hanks, 2014), average shear-wave velocity of 3500 m/s, and $R_{\phi\theta} = 0.63$ (Boore and Boatwright, 1984) to calculate the Brune velocity spectra ($v(f)$) in terms of moment (M_0) and corner frequency (f_c) for frequency bins between 1 and 35 Hz to constrain our inversion results

$$v_{\mathrm{CIE}}(f) = \frac{M_0 f_c}{1+\left(\frac{f}{f_c}\right)^2}. \qquad (3)$$

To identify the CIE, we seek an event with a source spectrum closest in shape to the theoretical Brune spectrum. This is the event with the smallest difference between its source spectrum, and the theoretical Brune spectrum, $v_{\mathrm{CIE}}(f)$, that is, the smallest L1 norm between 1 and 35 Hz. The constraint function ($C(f)$) is then the difference between our chosen CIE's demeaned observed source spectra and its theoretical Brune spectral shape for a stress drop of 5 MPa in each frequency bin:

$$C(f) = E_{\mathrm{CIE}}(f) - v_{\mathrm{CIE}}(f). \qquad (4)$$

The theoretical Brune spectrum we compute for the chosen constraint event is allowed to shift up or down, so that we identify the event with the best Brune spectral shape and not just the closest amplitude (Fig. 3).

We apply this constraint function to all event and site spectra in the dataset by subtracting it from each source spectra and adding it to each site spectra, in logarithmic space, thereby allowing the amplitude difference to serve as a relative baseline without significantly altering the shape of all other event and site spectra (Fig. 4), because our constraint method only assumes a Brune velocity spectrum for the CIE and allows the other events to preserve their shape. We find an event with magnitude 3.19 to have the best-fit Brune shape, with the chosen stress drop of 5 MPa (Fig. 2e).

We test our method by constraining the source and site spectra with various event spectra and find that the choice of

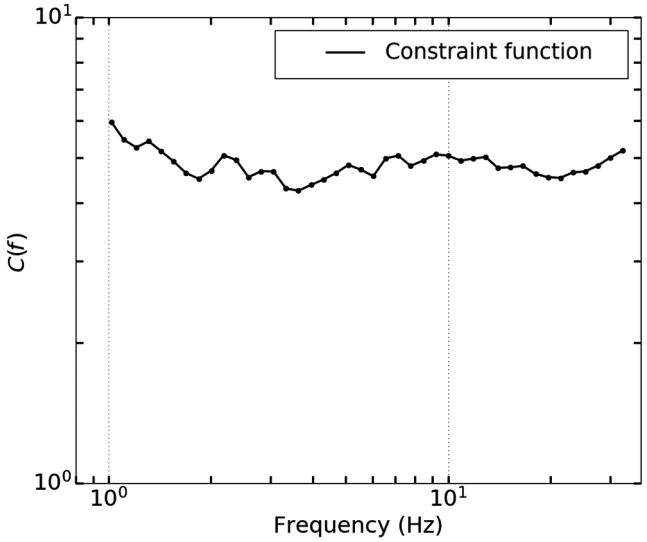

Figure 3. Method constraint function, that is, the difference between the event spectrum of the constraint identifying event and its Brune spectrum, plotted from 1 to 35 Hz.

constraint has little effect on our results. We also bootstrapped our sample by choosing random samples of source spectra of different sample sizes, and we find that our results are resistant to the choice of sample size. Our adaptation of the Andrews (1986) method yields source and site spectra from records of distinct events and/or recorded at different stations to be compared to each other without the need for the same reference station or constraining event.

Solving for Attenuation

Anderson and Hough (1984) define κ as the high-frequency shear-wave spectral decay of a record

$$A(f) = A_0 e^{-\pi f \kappa}, \tag{5}$$

in which $A(f)$ is the amplitude of the acceleration spectra at frequency f, and A_0 is the constant depending on source properties, epicentral distance, and other factors. κ, in this form, is a measure of attenuation over the entire path and at the site, with path κ a function of path distance (R), seismic quality factor (Q), and S-wave velocity (β)

$$\kappa = \left(\kappa_0 + \frac{R}{Q\beta}\right). \tag{6}$$

Anderson and Hough (1984) and following works (Hough *et al.*, 1988; Anderson, 1991) propose that κ is modeled with a site component and a path component as a function of distance

$$\kappa(R, S) = \kappa_0(S) + \tilde{\kappa}(R), \tag{7}$$

in which κ_0 is the attenuation at site S and $\tilde{\kappa}$ is the path attenuation as a function of epicentral distance R.

There have been many approaches to solving for site κ_0, including simply fitting equation (5) to an acceleration spectrum above the corner frequency, which usually only works for larger magnitude events with smaller corner frequencies. Another popular method is to fit a spectral shape as a function of source, path, and site parameters to a given record (Anderson and Humphrey, 1991 [AH] method). Often, κ given in equation (7) is measured as a function of distance, and then κ_0 is solved for at zero distance (i.e., Anderson, 1991).

In our study, we use the site spectra from our adapted Andrews (1986) inversion to directly calculate κ_0 for each site. We fit equation (5) for frequency bins between 1 and 35 Hz to each of our site spectra and set κ equal to site κ_0 with a generalize inverse solution. The frequency range is limited by long-period noise at the lower limit and the antialiasing filter applied at 35 Hz at the upper limit. The uncertainty on κ_0 is calculated from the uncertainty on the site spectra using the same least-squares inversion method. We assume the data covariance here to be the resulting data covariance from the inversion in the first step (decomposition of the spectra). We then obtain the covariance on κ_0 by propagating this error through with equation (5), given the pseudoinverse for this problem. Because the uncertainties on the site spectra are small, the uncertainties on κ_0 and A_0 are also small.

By calculating κ_0 from the site spectrum instead of the entire record spectrum, we avoid the challenge of solving for attenuation above the corner frequency, because all corner-frequency effects are put into the separate source spectra.

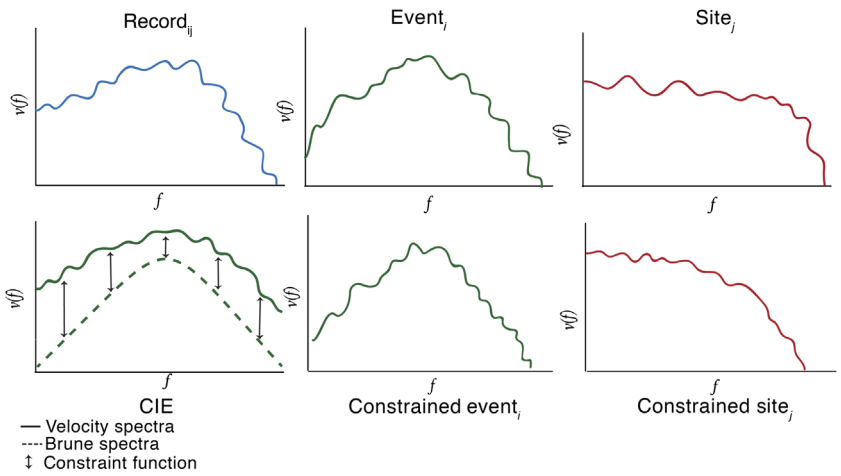

Figure 4. Cartoon depicting our event constraint methodology. A given record and its resulting event and site spectra after the inversion are shown in the top row. The difference between the event with the most "Brune-like" spectrum and its Brune spectrum is the constraint function (lower left). The constraint function is then applied to each event and site to constrain the missing degree of freedom. CIE, constraint identifying event. The color version of this figure is available only in the electronic edition.

Table 1
The Resulting Kappa, Amplification Values, and Uncertainties for Every Station in This Study, as Well as Kappa Values from Comparable Studies

	Spectral Amplitude (m)									κ(s)		
Site	κ_0 (s)	σ_{κ_0} (s)	σ_{κ_0} (% κ_0)	1–6 Hz	σ_{1-6}	6–14 Hz	σ_{6-14}	14–35 Hz	σ_{14-35}	Anderson (1991)	Kilb *et al.* (2012) AH*	Kilb *et al.* (2012) sfix*
BZN	0.034	1.424×10^{-4}	0.414	0.224	0.019	0.162	0.012	0.029	0.003	0.014	0.036	0.023
CPE	0.047	1.575×10^{-4}	0.332	0.347	0.036	0.173	0.016	0.026	0.003	—	—	—
CRY	0.041	1.328×10^{-4}	0.325	0.156	0.012	0.102	0.007	0.013	0.001	0.009	0.033	0.031
ERR	0.057	1.846×10^{-4}	0.325	0.945	0.076	0.374	0.025	0.048	0.005	—	—	—
FRD	0.050	2.440×10^{-4}	0.488	0.113	0.010	0.033	0.002	0.005	0.001	0.009	0.028	0.028
KNW	0.025	1.451×10^{-4}	0.581	0.101	0.008	0.077	0.005	0.027	0.003	0.002	0.023	0.008
LVA2	0.057	1.683×10^{-4}	0.295	0.240	0.019	0.075	0.005	0.008	0.001	0.028	0.041	0.038
PFO	0.017	1.492×10^{-4}	0.887	0.080	0.006	0.067	0.005	0.033	0.003	0.004	0.029	0.010
PMD	0.031	1.345×10^{-4}	0.439	0.108	0.008	0.115	0.007	0.019	0.002	—	—	—
RDM	0.025	1.386×10^{-4}	0.558	0.159	0.013	0.189	0.012	0.037	0.004	0.006	0.022	0.018
SMER	0.018	1.331×10^{-4}	0.724	0.113	0.009	0.122	0.007	0.039	0.003	—	—	—
SND	0.059	1.684×10^{-4}	0.283	0.360	0.028	0.085	0.006	0.009	0.001	0.023	0.047	0.043
SOL	0.052	1.877×10^{-4}	0.364	0.909	0.080	0.214	0.016	0.048	0.006	—	0.072	0.050
SWS	0.045	1.514×10^{-4}	0.339	0.335	0.028	0.158	0.012	0.023	0.002	—	—	—
TRO	0.036	1.412×10^{-4}	0.397	0.422	0.034	0.144	0.010	0.043	0.004	0.014	0.041	0.033
WMC	0.038	1.463×10^{-4}	0.381	0.348	0.028	0.176	0.012	0.032	0.003	0.021	0.043	0.028

Anderson and Humphrey (1991) (AH) method.
*The Kilb *et al.* (2012) κ-values shown here are the average of their two horizontal κ-values.

Another advantage of our method is that we calculate one value of κ_0 per site instead of averaging the site κ_0's from all records at a given site. A single site spectrum and κ_0 can tell us about the mean site behavior in common with all of our records at a site.

In the inversion we present here, the only path adjustment is for $1/R$ geometrical spreading. This method assumes that Q attenuation is constant over the study region and would be a constant value at each frequency in the inversion. So, if there are variations in Q over our region, it would likely be included in either the source or site spectra, though difficult to separate out. We assume that variations in Q are small, but in future work it may be worth solving for path Q. We treat regional crustal amplification in the same manner. It should be the same at every site, and we assume that it is removed by the inversion.

Throughout this study, we report correlation coefficients, p-values, and statistical power values for a variety of relationships to assess the usefulness of spectral parameters to describe site effects. The p-value or probability value is the probability that, given that the null hypothesis is true, the test statistic will have the same or greater value than the observed results. In our case, it would be the probability that uncorrelated data will produce a Pearson R equal to or greater than the Pearson R of our data. The statistical power is the probability that the test correctly rejects the null hypothesis when another hypothesis is true, given the number of observations and a prescribed significance level. A high statistical power means that there is a high probability the null hypothesis is correctly rejected, but it does not tell us which alternative hypothesis may be true. A low statistical power means there is a high probability of a false negative, failing to reject the null hypothesis when it is actually false.

Results

Site Spectra

We use the 16 site spectra from the constrained inversion to fit for site κ_0 and the average spectral levels in three frequency bands: 1–6 Hz, 6–14 Hz, and 14–35 Hz (Table 1; Ⓔ Fig. S1). Overall, the site spectra are very well behaved and show similarly shaped exponential decay, as expected. Goodness of fit is measured by averaging the L2 norm in logarithmic space

$$\mathrm{L2} = (\log(A_0 e^{-\pi f \kappa}) - \log(S(f)^2))^2 \qquad (8)$$

over each frequency bin. The L2 norm is calculated in log space to stay consistent with the inversion transformation to log space. Certain sites, ERR, KNW, and PFO, fit the κ_0 exponential decay very well, whereas other sites show a worse fit to the exponential decay function, due to site amplification at certain frequencies (CPE) or a more gradual rate of decay (FRD; Ⓔ Fig. S1). The values of κ_0 vary from 0.017 (PFO) to 0.059 s (SND) (Ⓔ Fig. S2). The sites show a wide range of low-frequency spectral amplitudes. In the 1–6 Hz frequency range, site ERR has an average amplitude of 0.945 m, whereas KNW has an average amplitude almost a factor of 10 smaller at 0.101 m.

Comparing our Site κ_0 to Previous Studies

To compare the consistency of our method of calculating site κ_0 to other methods, we compare our results to those of previous studies. Each study employed a different inversion method and different data, so we are likely comparing relative values of κ_0 (Table 1; Fig. 5). For each comparison, the correlation coefficient, p-value, and the statistical power given a significance level 0.05 are noted on the figure, as well as a one-to-one line to show how the overall κ_0 values compare to each other.

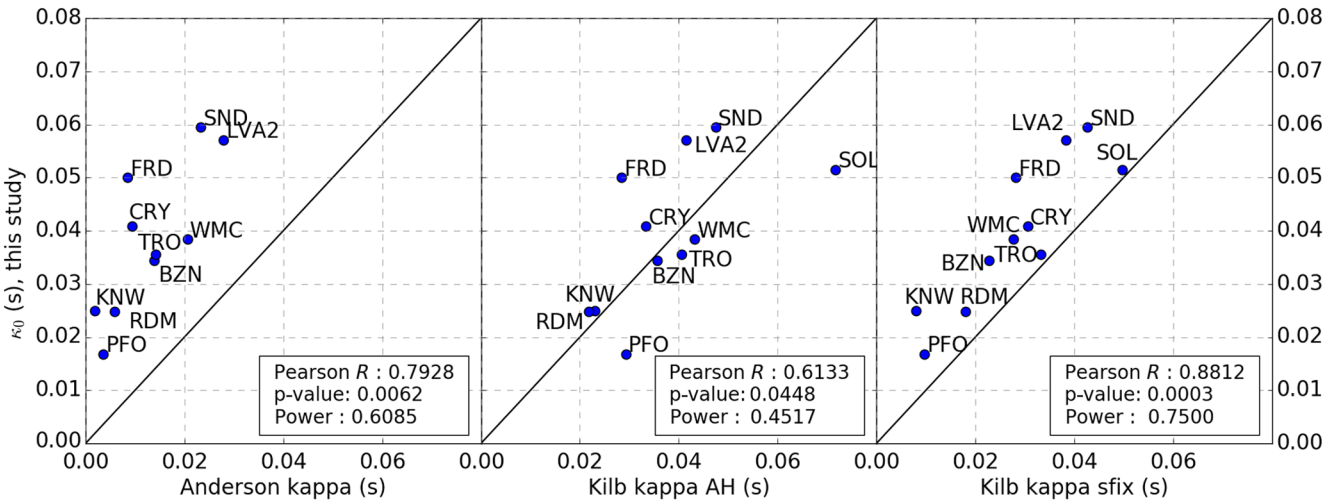

Figure 5. A comparison of our κ_0 values to three other previous studies for this region: (left) Anderson (1991) κ_0 values, (center) Kilb *et al.* (2012), Anderson and Humphrey (1991) (AH) method κ-values (here averaged between both horizontal components), and (right) Kilb *et al.* (2012) fixed stress-drop values (here averaged between both horizontal components). Note that for all sites the 1 sigma error bars are smaller than the plotted points. In all panels, each station is labeled on the plot, as well as the correlation coefficient (Pearson R), p-value, and statistical power assuming significance level of 0.05. The one-to-one line is plotted in black to compare overall values of κ_0. The color version of this figure is available only in the electronic edition.

Anderson (1991) published S-wave κ_0 values for 10 Anza stations in Southern California overlapping with the stations in our sample. Our κ_0 values are consistently higher than those of Anderson (1991), because all κ_0 values fall well above the one-to-one line. Our site κ_0s are larger than their Anderson (1991) counterparts by factors of 2.04 (LVA2) to 12.50 (KNW). Despite the offset between our κ_0 and Anderson κ_0, they show good correlation ($R = 0.7928$, $p = 0.0062$), and a relatively high statistical power (0.6085), meaning that it is likely a true positive result (Fig. 5).

Kilb *et al.* (2012) used various methods to calculate κ for stations in the ANZA network, including 11 of the stations in our sample. We compare our site κ_0 values those calculated with their AH method and fixed stress-drop method. The Kilb *et al.* (2012) AH method κ-values are more similar in overall value to ours than Anderson (1991) (Fig. 5), with κ-values falling close to the one-to-one line but with more scatter, so correlation is not as high. The relationship between our κ_0 values and the Kilb *et al.* (2012) fixed stress-drop κ is quite good. These show high correlation ($R = 0.8812$), a p-value below significance ($p = 0.0003$), and high statistical power (power = 0.75), suggesting that the results of these methods are more similar to each other than the previous two. As with the Anderson (1991) comparison, our κ_0s all fall above the one-to-one line, but differences are not as large, ranging from factors of 1.09 (TRO) to 3.13 (KNW) between our κ_0s and Kilb *et al.* (2012) fixed stress-drop κs.

Comparing Site Parameters to GMPE (PGA) Site Residuals

One possible application of site κ_0 and spectral amplitudes derived from our inversion site spectra is the inclusion of these site parameters into the site term of GMPEs (Laurendeau *et al.*, 2013; Ktenidou *et al.*, 2014). Currently, sites are typically represented by linear and nonlinear V_{S30} terms in GMPEs. However, V_{S30} only includes information about the top 30 m of a site, and in reality, a physically larger area may influence ground motion. To investigate the relationship between our site parameters and the GMPE site residuals, we compare our various site parameters to the empirical PGA GMPE site residuals of Sahakian *et al.* (2018). The GMPE was developed for small-magnitude earthquakes in southern California using a mixed-effects maximum-likelihood model following the form of Abrahamson *et al.* (2014) in which GMPE coefficients and site and event residuals are solved for simultaneously. Sahakian *et al.* (2018) found that the inclusion of V_{S30} did not improve their southern California regional GMPE, and they do not include it as a term in the GMPE. Instead, the empirical site residuals represent the contribution from the site on ground motions.

First, we compare V_{S30} and the GMPE site residuals for the 16 sites in our study. We find a low correlation coefficient ($R = 0.0448$) between the GMPE site residual and the site V_{S30} (natural log scale) for the 16 stations in our sample (Ⓔ Fig. S3). However, the p-value well above our significance level and low statistical power (0.0532) mean we have a high chance of falsely failing to reject the null hypothesis. Therefore, we cannot say if there exists or does not exist a relationship between the GMPE site residual and V_{S30} for our 16 stations. Similarly, we looked at these statistical measures for the stations with measured versus proxy V_{S30} values and find it similarly inconclusive; there are not enough sites with measured values of V_{S30} (we have only four) to determine whether the ambiguity is due to proxy values.

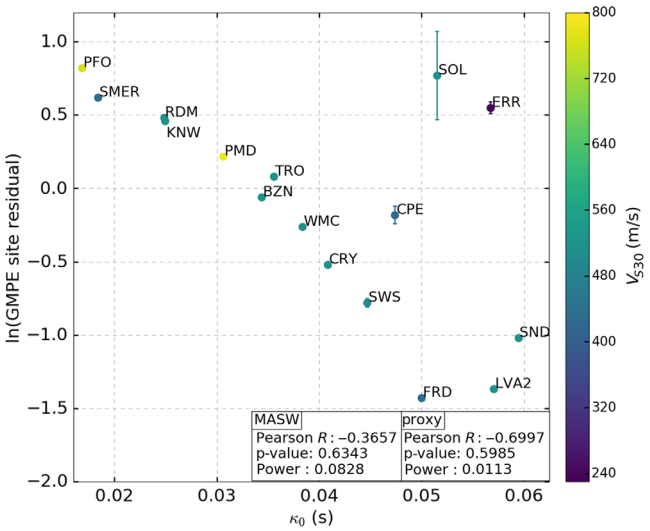

Figure 6. Ground-motion prediction equation (GMPE) site residual (Sahakian *et al.*, 2018) versus site κ_0 for the 16 stations in the study. 1 sigma error bars are plotted for the site residuals; however, for most sites, error bars are smaller than the points. Each station is labeled and shaded by V_{S30}. The correlation coefficient (Pearson R), p-value, and statistical power assuming a significance level of 0.05 are labeled for the multichannel analysis of surface waves (MASW) (ERR, PFO, PMD, SWS) and proxy (all other sites) V_{S30} method. For all 16 sites, the correlation coefficient is −0.6128, the p-value is 0.0116, and the power is 0.6302. The color version of this figure is available only in the electronic edition.

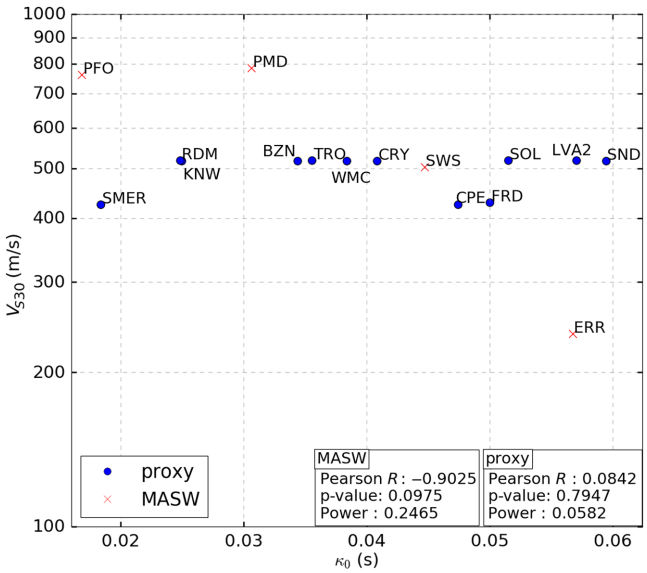

Figure 7. Site V_{S30} (natural log scale) versus site κ_0 for the 16 stations in the study. Station markers indicate V_{S30} proxy (dots) or measured V_{S30} via the MASW (crosses). Each station is labeled, as well as the correlation coefficient (Pearson R), p-value, and statistical power, assuming a significance level of 0.05 for the two methods. For all 16 sites, the correlation coefficient is −0.4700, p-value is 0.0975, and the power is 0.4208. The color version of this figure is available only in the electronic edition.

Including site attenuation as a term in GMPEs may provide a better representation of site response and reduce uncertainty. To test this idea, we compare site κ_0 to GMPE site residuals from a local southern California GMPE (Sahakian *et al.*, 2018) as an empirical estimate of site effects for the stations included in our study (Fig. 6). We find a negative correlation between site κ_0 and the GMPE site residuals ($R = -0.6128$). Without the two largest outliers (ERR and SOL) the correlation is much higher with an R-value of −0.9343. The small p-value and relatively high power means we likely correctly reject the null hypothesis, and there exists a relationship between the GMPE site residual and site κ_0.

We also compare site κ_0 to V_{S30} to investigate a possible relationship between near-surface velocity and attenuation, but we find only a weak negative correlation between site V_{S30} (natural log) and site κ_0 with a Pearson R-value of −0.4700 (Fig. 7). Again, a negative correlation is generally what we expect for the high frequencies considered here: larger V_{S30} values typically imply smaller amplitudes for high-frequency ground motion (i.e., Seyhan and Stewart, 2014), and larger κ_0 also implies smaller amplitudes. If we look at the relationship for only the sites with measured values of V_{S30}, the correlation improves ($R = -0.9025$), but with only four sites, the p-value and statistical power are too small to draw conclusions (p-value = 0.0975, power = 0.2465). Similarly, V_{S30} shows no relationship with spectral amplitudes (Ⓔ Fig. S4). There is higher correlation when we look at sites with measured V_{S30}, but again the p-value and power are small because of the small sample size.

Site characteristics can also be described by the site's average spectral amplitude over certain frequency ranges. Sites with stronger ground motion will have larger amplitude spectra. We compare the GMPE site residuals to our three spectral levels: 1–6 Hz, 6–14 Hz, and 14–35 Hz (Fig. 8). The two lower frequency ranges show low correlation between the GMPE site residual and spectral amplitude, but the higher frequency band shows a strong positive correlation ($R = 0.8426$) between the site residual and amplitude. This may indicate that the PGA used in Sahakian *et al.* (2018) is coming from this highest frequency band of 14–35 Hz, which is to be expected, given the small magnitudes of the data used in that study ($\mathbf{M} \sim 1$–3).

Discussion

Comparison with Anderson (1991) Site κ_0

Our site κ_0s are fairly similar to the Anderson site κ_0. Anderson (1991) calculated site attenuation by modeling κ_0 values from Hough *et al.* (1988) and Anderson and Hough (1984) as a distance-independent component $\kappa_0(S)$ and distance-dependent component $\tilde{\kappa}(R)$ for each site, as in equation (3). The values of κ_0 from Hough *et al.* (1988) and Anderson and Hough (1984) were determined by fitting earthquake spectra with the exponential decay function $A(f) = A_0 e^{-\pi f \kappa}$ in log–linear space over a frequency range above the corner frequency and below the frequency at which

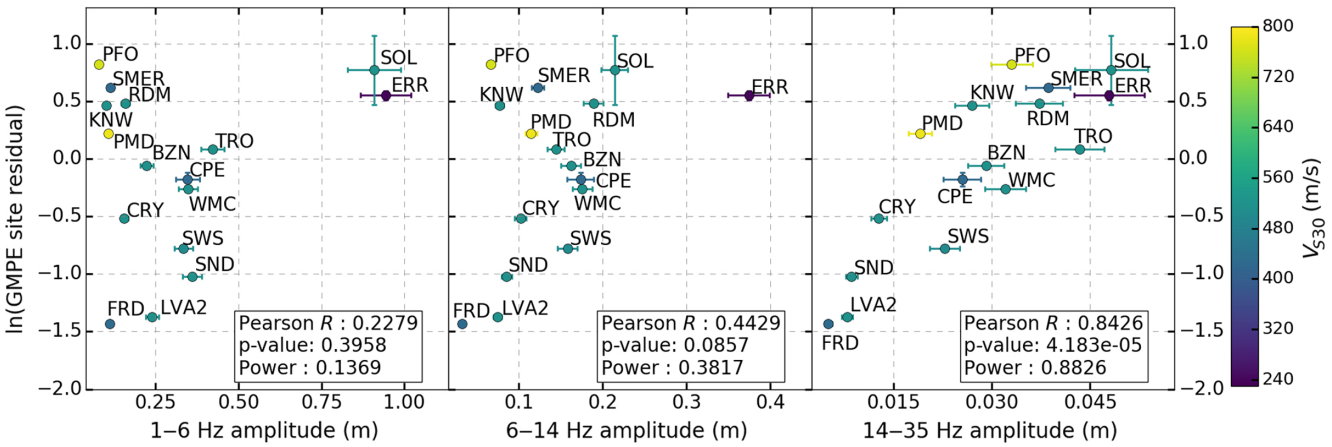

Figure 8. A comparison of the GMPE site residuals of Sahakian *et al.* (2018) to the site spectral amplitudes over three frequency ranges: (left) 1–6 Hz, (center) 6–14 Hz, and (right) 14–35 Hz. In all panels, each station is labeled on the plot, as well as the correlation coefficient (Pearson R), p-value, and statistical power, assuming a significance level of 0.05. 1 sigma error bars are plotted for both the spectral amplitudes and site residuals. The color version of this figure is available only in the electronic edition.

noise begins to dominate the signal, determined by eye to be 15–100 Hz for their study. Anderson (1991) assume no particular function of $\tilde{\kappa}(R)$, only that it is a smooth function of R. Removing the distance-dependent component of attenuation should result in an attenuation term, which comes solely from the site conditions. Anderson (1991) published P-wave and S-wave $\kappa_0(S)$ values for 11 stations, 10 of which overlap with the stations in our sample.

Although there is good correlation between our site κ_0s and the Anderson (1991) site κ_0s, we find that our values are consistently higher than those of Anderson (1991). The discrepancy in overall value between our site κ_0 and the Anderson (1991) site κ_0 could be due to corner-frequency effects in their method. The method of Anderson and Hough (1984) does not remove source contributions to their spectra; instead, they try to account for corner-frequency effects by fitting exponential decay above 15 Hz. The events in the sample of Anderson (1991) have magnitudes between 1.7 and 4.4, so the smallest events could likely have corner frequencies above 15 Hz, causing the corner frequency to be in the range in which they solve for κ_0. This could potentially cause their κ_0 values to appear to be smaller in value than the actual site attenuation, masked in part by corner frequency.

Comparison with Kilb AH and Fixed Stress-Drop κs

Our κ_0s are very similar to Kilb fixed stress-drop κ but have absolute values closer to κ AH. Kilb *et al.* (2012) used the AH method to solve for κ. The method fits each record spectra to model spectra with a Brune source and κ exponential decay

$$\ln[M(f_i, r)] = \ln(M_0) + \ln(A_0) - \pi\kappa f_i + \ln\left\{(2\pi f_i)^\gamma \left[1 + \left(\frac{f_i}{f_0}\right)^2\right]^{-1}\right\}. \quad (9)$$

They use a least-squares method to solve for earthquake moment, corner frequency, and κ for 41 earthquakes, $M_L > 3.5$ within 40 km of the ANZA network centroid. They determine that at these close distances, κ is dominated by the site, so they do not separate site and path κ. The fixed stress-drop method is the same, but the stress drop is fixed at a regional value of 4.7 MPa (Biasi and Anderson, 2007) and solved only for seismic moment and κ to investigate corner-frequency effects. They find that fixing the stress drop stabilizes the method by avoiding trade-offs between stress drop and corner frequency. They see tighter clustering in κ when stress drop is fixed, suggesting that variable corner frequency/numerical instability could be responsible for most of the κ spread (at a given site).

There is much more scatter between the results of this study and Kilb's AH κ, as opposed to the scatter between this study and their fixed stress-drop κ. This study systematically finds higher κ_0 than Kilb's fixed stress-drop κ, but because they fix the corner frequency and then solve for κ (instead of the site spectra themselves), it could be affected by the stress-drop value they assume. In other words, if Kilb *et al.* (2012) fixed the stress drop at a smaller value, they would force the last term of equation (4) to a smaller value, and the inversion would naturally partition more of the record amplitude into κ. This would adjust the fixed stress-drop values to be closer to ours, but the scatter would remain the same. We tested our method using a set of constraint events with a variety of stress drops (1.7–5 MPa, including 4.7 as in used in Kilb *et al.*, 2012) and find negligible changes in our resulting values of κ_0. Both Anderson (1991) and Kilb *et al.* (2012) use time windows of 5 s or less after the S-wave arrival

to compute κ, whereas we use a window of 62 s. The differing contributions from scattering could be another explanation for the discrepancy in our κ_0 values (Parolai *et al.*, 2015; Pilz and Fäh, 2017). It is unclear, however, if this would increase or decrease our values of κ_0, because this may be distance dependent (Aki and Chouet, 1975; Mai *et al.*, 2010; Mena *et al.*, 2010; Bydlon and Dunham, 2015; Sahakian *et al.*, 2019), and our recordings come from a range of source-to-site distances. Finally, the difference could perhaps be due to effects of site resonance influencing the inversion for κ_0 (Parolai and Bindi, 2004), but we believe that our frequency window is large enough that the influence of site resonance is likely very small.

Correlation between κ_0 and GMPE (PGA) Site Residuals

For the stations in our study, there is no evidence of a correlation between PGA–GMPE site residuals and V_{S30}. The high statistical power means that we have a high probability of a false negative, therefore we cannot definitively conclude that there is no relationship between site amplification and V_{S30} for these stations. Although it is inconclusive if V_{S30} correlates with empirical site effects, it is certain that there is a relationship between these site effects and κ_0. This confirms that, in this region and for our smaller magnitude events, κ_0 is likely a better measure of site effects for high-frequency ground motion for small-magnitude events than V_{S30} (Silva *et al.*, 1998; van Houtte *et al.*, 2011; Edwards *et al.*, 2015). We propose that κ_0 could be used in the future to remove site effects for PGA for seismological studies using similar small-magnitude southern California datasets.

The negative correlation we see between the empirical site effects and κ_0 agrees with what we expect: sites with small κ_0 values (less attenuating) relate to a positive GMPE site residual, and sites with large κ_0 values (more attenuating) have a negative GMPE site residual. A correlation between the GMPE residuals and site κ_0 may indicate that part of the site residual is due to unmodeled high-frequency site attenuation. Because the GMPE residual is the difference between observed ground motion and the predicted ground motion, a positive residual represents an underprediction by the GMPE, and a negative residual represents an overprediction by the GMPE. We expect that underpredicted ground motion corresponds to a more attenuating site than average.

Stations ERR and SOL appear to deviate slightly from the expected relation. The two stations have relatively high values of site κ_0 (more attenuating) and positive GMPE residuals (underpredicted ground motion), which is opposite to what we expect and the trends observed for the other stations. The outlying stations are two of the geographically farthest from the ANZA network centroid (SOL on the coast near San Diego and ERR in the Salton trough), so their high site κ_0 and positive GMPE site residuals could indicate a difference in site or path geology and warrant further study.

High-Frequency Spectral Amplitudes and GMPE Site Residuals

The GMPE site residuals do not show a relationship with site spectral amplitude levels for the 1–6 Hz and 6–14 Hz frequency ranges, but there is a positive relationship in the 14–35 Hz frequency range. This positive correlation is likely because of the high frequencies that contribute to PGA site residuals, for our relatively small-magnitude events. Because the frequency content of larger magnitudes would vary, further exploration is needed to determine how this relationship, and that between site residuals and κ_0, scale to larger magnitudes. Although we do not have empirical site amplification terms available to us for intensity measures other than PGA, this is a crucial next step in understanding if, and how, lower spectral amplitude levels could be used in estimating site effects for a wider range of magnitudes.

The Complexity of Site Effects

Our results suggest that site κ_0 and high-frequency spectral amplitudes are good proxies of site effects on PGA, in our magnitude range. Site κ_0 and spectral amplitude give a more physical description of site characteristics than does V_{S30}, in addition to including a larger site area than the arbitrary 30 m depth bound. Our results suggest that, for such magnitude ranges, κ_0 is a robust empirical estimate of site effects. Our method provides a full site spectrum that could be explored in future work for inclusion for ground-motion modeling and seismic hazard analysis. For applicability to hazard analyses, it will be crucial to fully understand the relationship between κ_0 and ground motions for larger-magnitude events. This will require either a larger database of events, or testing this same method in another region that has experienced larger earthquakes.

Conclusions

Our new approach of applying the Andrews (1986) inversion with a Brune event constraint yields useful site and source spectra. The site spectra allow for the calculation of site κ_0 and spectral amplitudes. We find that both site κ_0 and high-frequency site amplification correlates well with GMPE site residuals, indicating that they are both a good proxy of site effects on ground motion for the sites and magnitudes included in this study. In addition to studying site spectra, our method allows for the future study of source spectra (i.e., computation of stress drop).

Our preliminary results show that κ_0 is a promising measure of site effects on ground motion. As the engineering seismology community moves toward nonergodic ground-motion models, spatially varying models of κ_0 could be helpful for representing site effects. Future work is necessary to find how the relationship between κ_0 and site effects scale with earthquake magnitude, as well as determining the best method of incorporating κ_0 and site amplification into ground-motion models. Finally, this method does not

separate out path and site attenuation, in the form of crustal Q versus site attenuation. This is also an important consideration moving forward.

Data and Resources

These waveform data are publicly available and posted by the Scripps ANZA network on the Incorporated Research Institutions for Seismology (IRIS) Data Management Center (Southern California Earthquake Data Center [SCEDC], 2013) and by the California Institute of Technology (Caltech) network on the SCEDC (http://scedc.caltech.edu) and accessed from a local server. The event catalog was created with the U.S. Geological Survey (USGS) earthquake catalog website (https://earthquake.usgs.gov/earthquakes/search/). The authors used python to process and analyze the data and Generic Mapping Tools (GMT; Wessel and Smith, 1998) to create the map in Figure 1. The inversion code is available at https://github.com/aklimase/site_spectra. All websites were last accessed June 2017.

Acknowledgments

The authors would like to thank the U.S. Geological Survey (USGS) internal reviewers Eric Thompson and Tom Hanks for their thorough constructive feedback on this article. It greatly improved the article and brought up may important points for discussion. The authors thank journal reviewers Samantha Palmer and an anonymous reviewer for their time and comments on the article. This work was conducted under funding from Incorporated Research Institutions for Seismology (IRIS) summer internship program, a USGS and Pacific Gas & Electric (PG&E) funded student contract, and the University of Oregon Raymund Fellowship.

References

Abrahamson, N. A., W. J. Silva, and R. Kamai (2014). Summary of the ASK14 ground motion relation for active crustal regions, *Earthq. Spectra* **30,** no. 3, 1025–1055.

Aki, K., and B. Chouet (1975). Origin of coda waves: Source, attenuation, and scattering effects, *J. Geophys. Res.* **80,** no. 23, 3322–3342.

Allmann, B. P., and P. M. Shearer (2009). Global variations of stress drop for moderate to large earthquakes, *J. Geophys. Res.* **114,** no. B01310, doi: 10.1029/2008JB005821.

Anderson, J. G. (1991). A preliminary descriptive model for the distance dependence of the spectral decay parameter in southern California, *Bull. Seismol. Soc. Am.* **81,** 2186–2193.

Anderson, J. G., and S. E. Hough (1984). A model for the shape of the Fourier amplitude spectrum of acceleration at high frequencies, *Bull. Seismol. Soc. Am.* **74,** 1969–1993.

Anderson, J. G., and J. R. Humphrey Jr. (1991). A least-squares method for objective determination of earthquake source parameters, *Seismol. Res. Lett.* **62,** 201–209.

Andrews, D. J. (1986). Objective determination of source parameters and similarity of earthquakes of different size, in *Earthquake Source Mechanics*, S. Das, J. Boatwright, and C. H. Scholz (Editors), Am. Geophys. Union, Washington, D.C.

Aster, R. C., B. Borchers, and C. H. Thurber (2004). *Parameter Estimation and Inverse Problems*, Elsevier, Boston, Massachusetts.

Atkinson, G., and W. Silva (2000). Stochastic modeling of California ground motions, *Bull. Seismol. Soc. Am.* **90,** 255–274, doi: 10.1785/0119990064.

Baltay, A. S., and T. C. Hanks (2014). Understanding the magnitude dependence of PGA and PGV in NGA-West2 Data, *Bull. Seismol. Soc. Am.* **104,** no. 6, doi: 10.1785/0120130283.

Berger, J., L. M. Baker, J. N. Brune, J. B. Fletcher, T. C. Hanks, and F. L. Vernon (1984). The Anza array: A high-dynamic, range, broadband, digitally radiotelemetered seismic array, *Bull. Seismol. Soc. Am.* **74,** no. 4, 1469–1481.

Biasi, G. P., and J. G. Anderson (2007). Measurement of the parameter kappa, and reevaluation of kappa for small to moderate earthquakes at seismic stations in the vicinity of Yucca Mountain, Nevada, *Final Technical Report TR-07-007*, Nevada System of Higher Education (NSHE), University of Nevada, Las Vegas (UNLV), 232 pp, doi: 10.2172/920643

Boatwright, J., J. B. Fletcher, and T. E. Fumal (1991). A general inversion scheme for source, site, and propagation characteristics using multiply recorded sets of moderate-sized earthquake, *Bull. Seismol. Soc. Am.* **81,** no. 5, 1754–1782.

Boore, D. M., and J. Boatwright (1984). Average body-wave radiation coefficients, *Bull. Seismol. Soc. Am.* **74,** 1615–1621

Brune, J. N. (1970). Tectonic stress and the spectra of seismic shear waves from earthquakes, *J. Geophys. Res.* **75,** no. 26, 4997–5009, doi: 10.1029/JB075i026p04997.

Brune, J. N. (1971). Correction [to "Tectonic Stress and the Spectra of Seismic Shear Waves from Earthquakes"], *J. Geophys. Res.* **76,** 5002, doi: 10.1029/JB076i020p05002.

Bydlon, S. A., and E. M. Dunham (2015). Rupture dynamics and ground motions from earthquakes in 2-D heterogeneous media, *Geophys. Res. Lett.* **42,** 1701–1709, doi: 10.1002/2014GL062982.

California Institute of Technology (Caltech) (1926). Southern California Seismic Network, *International Federation of Digital Seismograph Networks*, Other/Seismic/Network, doi: 10.7914/SN/CI.

Castro, R. R., J. G. Anderson, and S. K. Singh (1990). Site response, attenuation and source spectra of *S* waves along the Guerrero, Mexico, subduction zone, *Bull. Seismol. Soc. Am.* **80,** 1481–1503.

Derras, B., P. Y. Bard, and F. Cotton (2016). Site-condition proxies, ground motion variability, and data-drive GMPEs: Insights from the NGA-West2 and RESORCE datasets, *Earthq. Spectra* **32,** no. 4, 2027–2056.

Derras, B., P. Y. Bard, and F. Cotton (2017). V_{S30}, slope, H_{800}, and f_0: Performance of various site-condition proxies in reducing ground-motion aleatory variability and predicting nonlinear site response, *Earth Planets Space* **69,** no. 1, 133.

Douglas, J. (2002). Earthquake ground motion estimation using strong-motion records: A review of equations for the estimation of peak ground acceleration and response spectral ordinates, *Earth Sci. Rev.* **61,** 43–104, doi: 10.1016/S0012-8252(02)00112-5.

Edwards, B., O.-J. Ktenidou, F. Cotton, N. Abrahamson, C. Van Houtte, and D. Fäh (2015). Epistemic uncertainty and limitations of the κ_0 model for near-surface attenuation at hard rock sites, *Geophys. J. Int.* **202,** no. 3, 1627–1645.

Gallipoli, M. R., and M. Mucciarelli (2009). Comparison of site classification from V_{S30}, V_{S10}, and HVSR in Italy, *Bull. Seismol. Soc. Am.* **99,** no. 1, 340–351.

Hough, S. E., J. G. Anderson, J. Brune, F. Vernon III, J. B. Fletcher, L. Haar, and L. Baker (1988). Inverting for attenuation, *Bull. Seismol. Soc. Am.* **78,** 672–691.

Kilb, D., G. Biasi, J. Anderson, J. Brune, Z. Peng, and F. L. Vernon (2012). A comparison of spectral parameter kappa from small and moderate earthquakes using southern California ANZA seismic network data, *Bull. Seismol. Soc. Am.* **102,** no. 1, 284–300.

Ktenidou, O.-J., F. Cotton, N. A. Abrahamson, and J. Anderson (2014). Taxonomy of *k*: A review of definitions and estimation approaches targeted to applications, *Seismol. Res. Lett.* **85,** 135, doi: 10.1785/0220130027.

Laurendeau, A., F. Cotton, O.-J. Ktenidou, L. F. Bonilla, and F. Hollender (2013). Rock and stiff-soil amplification: Dependency on V_{S30} and kappa (κ_0), *Bull. Seismol. Soc. Am.* **103,** no. 6, 3131–3148.

Mai, P. M., W. Imperatori, and K. B. Olsen (2010). Hybrid broadband ground-motion simulations: Combining long-period deterministic synthetics with high-frequency multiple S-to-S backscattering, *Bull. Seismol. Soc. Am.* **100,** no. 5A, 2124–2142, doi: 10.1785/0120080194.

Mena, B., P. M. Mai, K. B. Olsen, M. Purvance, and J. Brune (2010). Hybrid broadband ground motion simulation using scattering Green's

functions: Application to large magnitude events, *Bull. Seismol. Soc. Am.* **100,** no. 5A, 2143–2162, doi: 10.1785/0120080318.

Oth, A., D. Bindi, S. Parolai, and D. D. Giacomo (2011). Spectral analysis of K-NET and KIK-net data in Japan, part II: On attenuation characteristics, source spectra, and site response of borehole and surface stations, *Bull. Seismol. Soc. Am.* **101,** 667–687.

Parolai, S., and D. Bindi (2004). Influence of soil-layer properties on k evaluation, *Bull. Seismol. Soc. Am.* **94,** no. 1, 349–356.

Parolai, S., D. Bindi, and M. Pilz (2015). κ_0: The role of intrinsic and scattering attenuation, *Bull. Seismol. Soc. Am.* **105,** no. 2A, 1049–1052.

Pilz, M., and D. Fäh (2017). The contribution of scattering to near-surface attenuation, *J. Seismol.* **21,** no. 4, 837–855.

Prieto, G. A., R. L. Parker, D. J. Thomson, F. L. Vernon, and R. L. Graham (2007). Reducing the bias of multitaper spectrum estimates, *Geophys. J. Int.* **171,** 1269–1281.

Prieto, G. A., R. L. Parker, and F. L. Vernon (2009). A Fortran 90 library for multitaper spectrum analysis, *Comp. Geosci.* **35,** pp. 1701–1710, doi: 10.1016/j.cageo.2008.06.007.

Sahakian, V. J., A. S. Baltay, T. C. Hanks, J. Buehler, F. L. Vernon, D. Kilb, and N. Abrahamson (2018). Decomposing leftovers: Event, path, and site residuals for a small magnitude ANZA region GMPE, *Bull. Seismol. Soc. Am.* **108,** 2478–2492, doi: 10.1785/0120170376.

Sahakian, V. J., A. S. Baltay, T. C. Hanks, J. Buehler, F. L. Vernon, D. Kilb, and N. Abrahamson (2019). Ground-motion residuals, path effects, and crustal properties: A pilot study in Southern California, *J. Geophys. Res.* **124,** no. 6, 5738–5753.

Seyhan, E., and J. P. Stewart (2014). Semi-empirical nonlinear site amplification from NGA-West 2 data and simulations, *Earthq. Spectra* **30,** no. 3, 1241–1256, doi: 10.1193/063013EQS181M.

Silva, W., R. Darragh, N. Gregor, G. Martin, N. Abrahamson, and C. Kircher (1998). Reassessment of site coefficients and near-fault factors for building code provisions, *Technical Report Program Element II: 98-HQ-GR-1010*, Pacific Engineering and Analysis.

Silva, W. J., and R. B. Darragh (1995). Engineering characterization of strong ground motion recorded at rock sites, *Calif., Report No. TR-102262*, Electric Power Research Institute, Palo Alto, California.

Southern California Earthquake Data Center (SCEDC) (2013). Southern California Earthquake Data Center, *Caltech. Dataset*, doi: 10.7909/C3WD3xH1.

Thompson, E., and D. Wald (2016). Uncertainty in V_{S30}-based site response, *Bull. Seismol. Soc. Am.* **106,** no. 2, 453–463.

Thomson, D. J. (1982). Spectrum estimation and harmonic analysis, *Proc. IEEE* **70,** 1055–1096.

Trugman, D. T., and P. M. Shearer (2018). Strong correlation between stress drop and peak ground acceleration for recent M 1–4 earthquakes in the San Francisco Bay Area, *Bull. Seismol. Soc. Am.* **108,** no. 2, 929–945, doi: 10.1785/0120170245.

Van Houtte, C., S. Drouet, and F. Cotton (2011). Analysis of the origins of κ (kappa) to compute hard rock to rock adjustment factors for GMPEs, *Bull. Seismol. Soc. Am.* **101,** no. 6, 2926–2941.

Van Houtte, C., O.-J. Ktenidou, T. Larkin, and C. Francois-Holden (2014). Hard-site 0 (Kappa) calculations for Christchurch, New Zealand, and comparison with local ground-motion prediction models, *Bull. Seismol. Soc. Am.* **104,** 1899–1913, doi: 10.1785/0120130271.

Vernon, F. L. (1989). Analysis of data recorded on the ANZA seismic network, *Ph.D. Thesis*, University of California, San Diego.

Wessel, P., and W. H. Smith (1998). New, improved version of generic mapping tools released, *Eos Trans. AGU* **79,** no. 47, 579.

Yong, A., S. E. Hough, J. Iwahashi, and A. Braverman (2012). A terrain-based site-conditions map of California with implications for the contiguous United States, *Bull. Seismol. Soc. Am.* **102,** no. 1, 114–128.

Yong, A., E. M. Thompson, D. Wald, K. L. Knudsen, J. K. Odum, W. J. Stephenson, and S. Haefner (2016). Compilation of V_{S30} data for the United States, *U.S. Geol. Surv. Data Series 978*, 8 pp., doi: 10.3133/ds978.

Alexis Klimasewski
Annemarie Baltay
John Boatwright
Jon B. Fletcher
Lawrence M. Baker
U.S. Geological Survey
Earthquake Science Center
345 Middlefield Road, MS 977
Menlo Park, California 94025 U.S.A.
aklimase@uoregon.edu

Valerie Sahakian
Department of Earth Sciences
100 Cascade Hall, 1272
University of Oregon
Eugene, Oregon 97403 U.S.A.

Manuscript received 17 February 2019;
Published Online 10 September 2019